JOURNAL OF GEOPHYSICAL RESEARCH, VOL. 111, B08101, doi:10.1029/2005JB003657, 2006

The rise and fall of axial highs during ridge jumps

Anjana K. Shah[1,2] and W. Roger Buck[1]

Received 30 January 2005; revised 11 March 2006; accepted 13 April 2006; published 17 August 2006.

[1] We simulate jumps of ocean spreading centers with axial high topography using elastoplastic thin plate flexure models. Processes considered include ridge abandonment, the breaking of a stressed plate on the ridge flank, and renewed spreading at the site of this break. We compare model results to topography at the East Pacific Rise between 15°25′N and 16°N, where there is strong evidence of a recent ridge jump. At an apparently abandoned ridge, gravity data do not suggest buoyant support of topography. Model deflections during cooling and melt solidification stages of ridge abandonment are of small vertical amplitude because of plate strengthening, resulting in the preservation of a ''frozen'' fossil high. The present-day high is bounded by slopes with up to a 40% grade, a scenario very difficult to achieve flexurally given generally accepted constraints on lithospheric strength. We model these slopes by assuming that the height at which magma is accreted increases rapidly after the ridge jumps. This increase is attributed to high overburden pressure on melt that resided in an initially deep magma chamber, followed by a rapid increase in temperature and melt supply to the region shortly after spreading began. The high is widest at the segment center, suggesting that magmatic activity began near the center of the segment, propagated south and then north. The mantle Bouguer anomaly exhibits a ''bull's-eye'' pattern centered at the widest part of the high, but the depth of the axis is nearly constant along the length of the segment. We reconcile these observations by assigning different cross-axis widths to a low-density zone within the crust.

Citation: Shah, A. K., and W. R. Buck (2006), The rise and fall of axial highs during ridge jumps, *J. Geophys. Res.*, *111*, B08101, doi:10.1029/2005JB003657.

1. Introduction

[2] Tectonic plates move smoothly over fluid-like mantle over timescales of millions of years, as indicated by seafloor magnetic anomalies and geodetic measurements. However, there are many indicators that plate boundaries are not steady state features. Changes in the position and orientation of plate boundaries take place in the form of ridge propagation, ridge migration and ridge jumps. There is evidence that these phenomena are associated with larger-scale changes in spreading direction [*Hey*, 1977], thus depending on far field lithospheric stresses, but other evidence that they are affected by the presence of hot spots or smaller plumes [*Hey*, 1979; *Mammerickx*, 1984], thus depending on regional mantle processes. In the latter case, studies have suggested that the presence of a plume can weaken the lithosphere and perhaps generate aesthenospheric flow, leading to a rearrangement of upwelling patterns [*Morgan*, 1978; *Schilling*, 1985, 1991; *Sleep*, 1992; *Small*, 1995]. Both mechanisms affect processes in the ocean crust, requiring the cessation of spreading and melt production at one locale, and initiation of these processes at another.

[3] Numerous basic questions aside from causality surround ridge jumps and the associated physical processes. How is topography supported at an abandoned ridge if the associated thermal and melt structure no longer exist? When spreading begins at the new location, does it start vigorously, perhaps fed by a nearby plume, or does it develop gradually, as the nearby environment may be relatively cold? As old lithosphere is heated and then broken, what are the effects on axial morphology?

[4] These processes depend much on the thermal and melt structure of the crust and mantle, and must be considered in light of recent results: seismic and compliance data [*Dunn and Toomey*, 2000; *Crawford et al.*, 1999] and models of axial high topography [*Shah and Buck*, 2001] suggest the presence of melt within the lower crust beneath the ridge axis at fast spreading centers; and both seismic [*Forsyth et al.*, 1998] and modeling [*Eberle et al.*, 1998] efforts suggest that melt in the mantle is not focused within a narrow mantle column as inferred from earlier models of axial high topography and gravity data [*Wang and Cochran*, 1993; *Magde et al.*, 1995; *Wilson*, 1992].

[5] We use flexural models predicting topography and gravity to constrain the thermal and melt regimes at a portion of the East Pacific Rise (EPR) which has recently experienced a ridge jump. *Shah and Buck* [2003] developed

[1]Lamont-Doherty Earth Observatory, Columbia University, Palisades, New York, USA.
[2]Now at Applied Signal Technology, Arlington, Virginia, USA.

0148-0227/06/2005JB003657$09.00

models that predict the changes in deflection of lithosphere as it moves away from the ridge axis that depend on steady state thermal conditions in the crust, and incorporate the effects of plastic yielding associated with faulting. These models allow curvature to develop at the ridge axis as described by *Buck* [2001]. We further develop these models to allow for temporal changes in thermal and magmatic conditions and the position of the ridge axis. We model the stages of a ridge jump, including abandonment of an active spreading center, the breaking apart of older, stressed lithosphere at a new ridge axis position, and subsequent spreading and accretion there.

[6] To constrain the models, we use data from the East Pacific Rise north of the Orozco fracture zone, 15°25′–16°N. This ridge, adjacent to a seamount chain, appears to have recently experienced a jump in its axis position [*Weiland and Macdonald*, 1996; *Carbotte et al.*, 2000]. A wealth of data are available for this region, including bathymetry, gravity, magnetic field, seismic reflection data, and basalt samples. We also qualitatively compare model results to other regions which have experienced a ridge jump over different timescales/space scales.

2. Data

2.1. East Pacific Rise, 15–16°N

[7] The East Pacific Rise between 15°25′N and 16°N (Figure 1) is a particularly well-surveyed region. *Weiland and Macdonald* [1996] conducted initial bathymetry, gravity, and magnetic field studies of the area. Later, *Carbotte et al.* [2000] conducted a seismic reflection survey, and refined bathymetry and gravity coverage. Preliminary geochemical studies have been preformed [*Langmuir et al.*, 1998]. The following is a synopsis of these studies.

[8] Along the length of the ridge, the axis lies at a nearly uniform depth of 2320 m, while the width of the high varies from 4 to 10 km. The segment is rather unusual in that the axis sits ~600 m above the surrounding flanks, instead of a more typical ~400 m observed elsewhere, it has a very flat crest and extremely steep sides (Figure 2), and it is substantially wider than elsewhere on the EPR (see *Scheirer and Macdonald* [1993] for a comparison of cross-sectional area). Slopes bounding the high are steep enough to reach nearly a 30% grade in various places (slope of 3:10). Such slopes are atypical of flexural deflections of mid-ocean ridge lithosphere, noting that to achieve a flexural wavelength of 2–3 km, a very weak elastic plate with an effective thickness ~200–400 m is required. Reflection seismic data suggest that the steep slopes do not represent fault scarps as there is no evidence of slip at depth, nor do they consist of extrusive pileup, as the base of layer 2A also shows similar slopes (Figure 2).

[9] Initial studies of magnetic lineations revealed asymmetric spreading, leading *Weiland and Macdonald* [1996] to postulate a ridge jump toward the west within the last 0.7 Ma. About 7–10 km east of the southern half of the axis, *Carbotte et al.* [2000] imaged a 300-m-high ridge distinctly different from abyssal hill fabric, striking parallel to the axis. They proposed that this is the abandoned ridge associated with the ridge jump, and thus constrain the timing of the jump to 0.3–0.15 Ma. This feature extends northward to ~15°50′N, where it meets slightly curved abyssal hill fabric. The source of this fabric, whose curvature resembles features observed at overlapping spreading centers, is uncertain. Farther north, this fabric straightens and resembles the abandoned ridge to the south, suggesting it may be a continuation of this feature.

[10] The present-day axial high is widest toward its center, at 15°40′–15°45′. Here the sides of the high climb higher than the present-day axis, forming cross-axis profiles which somewhat resemble bat ears. Seismic reflection surveys reveal that the "ears" are composed entirely of layer 2A. Near the base of the high, layer 2A thickens tremendously, up to nearly 1 km in places. Bathymetric studies led *Carbotte et al.* [2000] to postulate that a volcano or seamount was initially present at the locale, and was split by subsequent plate spreading. This volcano may have been related to the Mudskipper seamount chain, which lies less than 20 km west of the ridge segment. The proximity of this chain to the ridge axis suggests that the ridge may be plume-influenced. Preliminary geochemical measurements show mostly uniform basalt chemistry along-axis, with exception of a region of fresh glass sampled near 15°55′N. There is some suggestion that the basalts along the segment are from a slightly enriched source (e.g., K/Ti = 0.15) [*Langmuir et al.*, 1998].

[11] Using additional gravity data collected by *Carbotte et al.* [2000], we refined the mantle Bouguer anomaly (MBA) calculation of *Weiland and Macdonald* [1996] (Figure 1). The MBA near 16°N shows a marked bull's-eye pattern centered where the high is widest. At various mid-ocean ridges, especially the Mid-Atlantic Ridge, bull's-eye gravity anomalies have been attributed to variations in crustal thickness [e.g., *Lin et al.*, 1990]. *Weiland and Macdonald* [1996] determined that if the MBA low in the study area is due entirely to crustal thickening, the crust must be 2 km thicker in the bull's-eye region. Such thickness variations should produce a significant variation in along-axis depth due to density compensation; however the along-axis depth is nearly uniform along the 45+ km length of the ridge, including the areas where the MBA varies the most. Furthermore, where intermittent Moho reflectors from reflection seismics study are present, they do not seem to indicate deepening to this extent (S. Carbotte, personal communication, 2001). This suggests that the along-axis gravity variation has some other source. The Bouguer anomaly low is somewhat asymmetric, tapering more gradually over the southern part of the study area, over the abandoned ridge (Figure 3).

2.2. Other Areas

[12] Steep sides of axial highs have also been observed at other regions of the mid-ocean ridge system. This includes part of the East Pacific Rise between 8°30′N and 8°50′N [*Carbotte and Macdonald*, 1992] and the Southeast Indian Ridge (SEIR) near 107°30′E [*Cochran et al.*, 1997; *Sempéré et al.*, 1997]. This part of the SEIR also shows a bull's-eye gravity anomaly, and several seamounts nearby. It is currently unknown whether these highs have experienced recent ridge jumps, but at the EPR 8°30′–8°50′N, the Brunhes magnetic reversals lie at different distances from either side of the axis.

[13] *Mammerickx and Sandwell* [1986] studied several regions which had experienced ridge jumps, though over

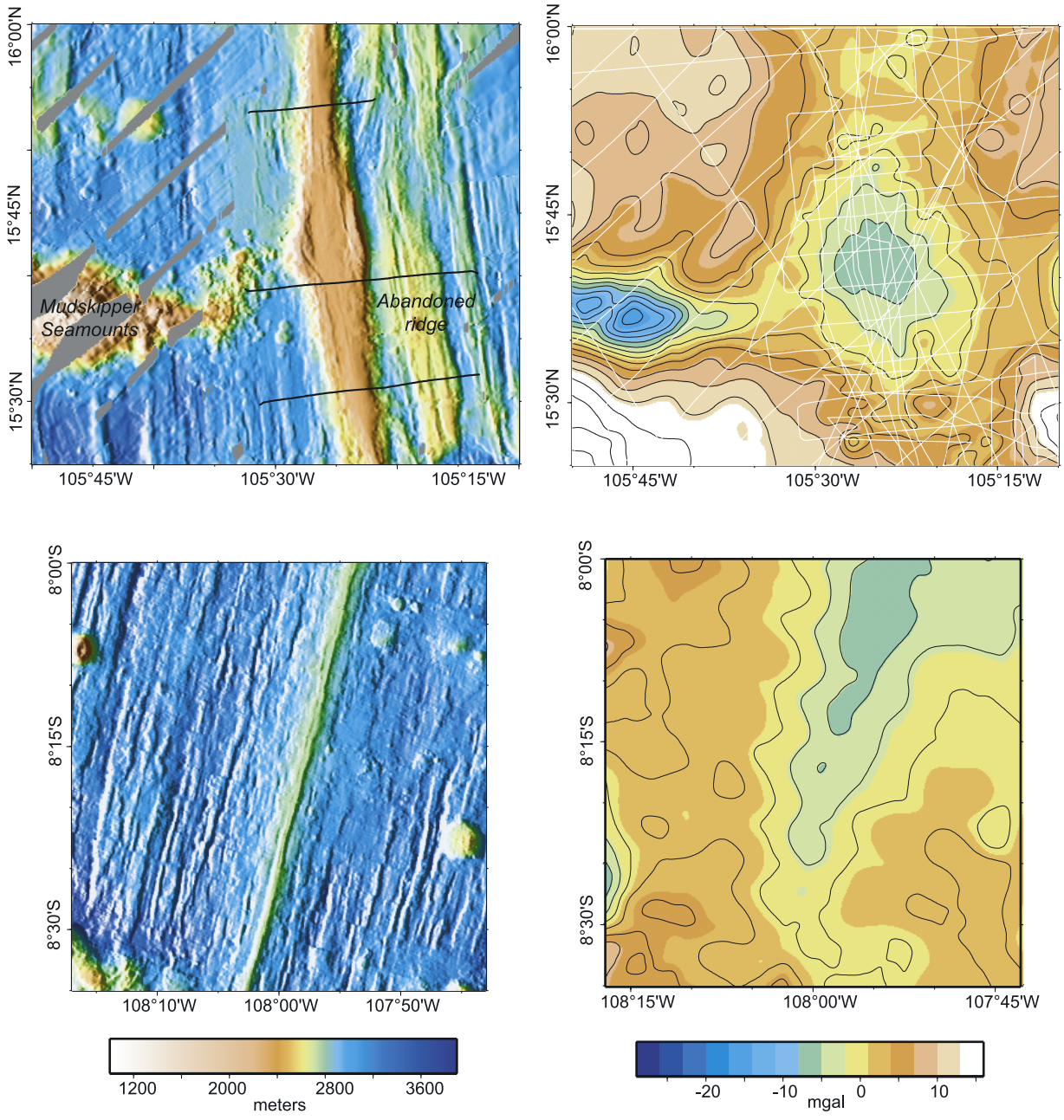

Figure 1. (left) Bathymetry of the EPR near (top) 16°N and (bottom) 8°S. Bold lines show locations of profiles in Figure 2. The rise at 16°N is particularly shallow, flat topped, and steep sided. An abandoned ridge sits 8–10 km east of the axis, while the Mudskipper seamounts are less than 20 km away from the axis to the west. The EPR at 8°S represents more typical East Pacific Rise morphology. (right) Mantle Bouguer anomalies for (top) 16°N and (bottom) 8°S with contour interval 2.5 mGal. A bull's-eye pattern marks 16°N, whereas a more linear pattern marks 8°S. White lines (top plot) show ship tracks where gravity data were collected. EPR 8°S data are from the RIDGE Multibeam Synthesis (bathymetry) and courtesy of J. Cochran (gravity). EPR 16°N data are courtesy of S. Carbotte.

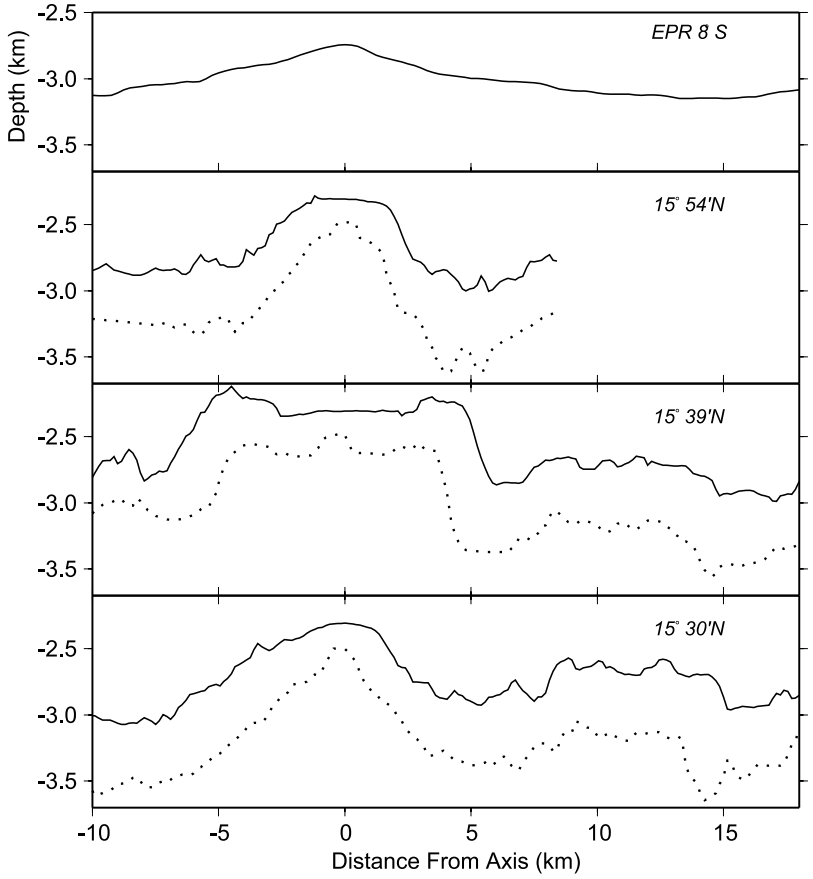

Figure 2. Cross-axis bathymetric profiles from the EPR at 8°S and various parts of the segment at 16°N (solid lines), and seismic layer 2A depth estimates (dashed lines). Layer 2A data are from *Carbotte et al.* [2000].

much greater spatial scales and thus timescales than our focus area near 16°N. These jumps have taken place some time ago, and illustrate the type of topography which may evolve some time after a ridge jump has occurred (Figure 4). In particular, we note steep slopes present near distances of 300 km and 1200 km, where the jump initiated.

3. Model Formulation

3.1. Flexure With Plastic Yielding

[14] To model ridge jumps, we use an incremental version of the thin plate flexure equation, following *Shah and Buck* [2001]. As the plate moves a distance Δx,

$$\frac{d^2(Dd^2\Delta w/dx^2)}{dx^2} + \Delta\rho g \Delta w = \Delta q, \tag{1}$$

where $\Delta w(x)$ is the change in plate deflection corresponding to a change in load $\Delta q(x) = q(x + \Delta x) - q(x)$. $D(x)$ is the plate rigidity, and $\Delta\rho$ the density contrast between the lithosphere and water. For this study, we consider nonsteady state boundary conditions. Although we assume that the axis remains in local isostasy, we allow conditions at depth to change over time, which in turns allows $w(0)$ to vary over time. We also allow for gradual changes in thermal structure and melt content with each step of the model, so that Δq may change with each incremental step Δx.

[15] We include the effects of plastic yielding due to bending stresses via a yield strength envelope, such as used by *Bodine et al.* [1981]. Generally, changes in stress depend on changes in curvature, as in elastic models, but are adjusted so that the total stress always remains within a yield strength envelope, whose extensional and compressional boundaries are defined, respectfully, as

$$\begin{aligned}\sigma_e &= -2\mu\rho g z/\left((1+\mu^2)^{1/2} + \mu\right)\\ \sigma_c &= 2\mu\rho g z/\left((1+\mu^2)^{1/2} - \mu\right),\end{aligned} \tag{2}$$

where μ is the friction coefficient, ρ is the density of the crust, and z is positive downward. Changes in stress are also adjusted so that the average change in stress over a column is always equal to zero. Given stress profiles $\sigma(x, z)$ over the plate thickness h at each incremental step, the rigidity is defined as the change in moment arising from the change in bending stress divided by the change in curvature

$$D(x) = \frac{\Delta M(x)}{\Delta w''(x)} = \frac{\int_0^h \sigma(x,z)z dz - \int_0^h \sigma(x-\Delta x,z)z dz}{\Delta w''(x)}. \tag{3}$$

The use of a yield strength envelope with an incremental flexural formulation is described in detail by *Shah and Buck* [2003].

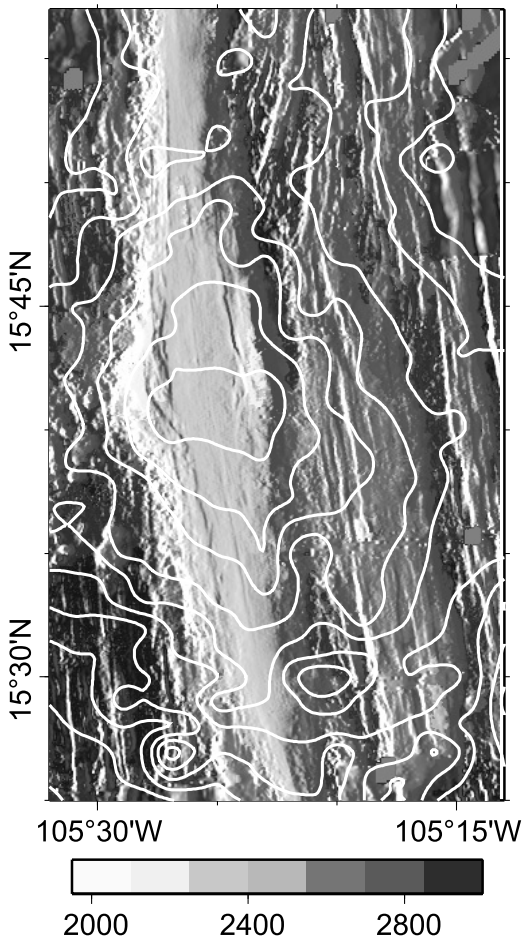

Figure 3. Bathymetry of the EPR axis and abandoned ridge near 16°N overlain with MBA contours (2 mGal interval) shown in Figure 1.

3.2. Thermal Structure

[16] We parameterize thermal and lithospheric structure similarly to *Shah and Buck* [2003]. We assume that temperatures increase linearly with depth to a maximum of 1200°C, approximating melt temperatures in the crust. A fraction of this depth (parameter *f*), starting at the top of the crust, is set to a uniform temperature of 200°C to mimic hydrothermal circulation effects. The base of the lithosphere is set to coincide with the 700°C isotherm [e.g., *Hirth et al.*, 1998].

[17] For a distance of x_0 from the axis, the temperatures are kept uniform such that the 1200°C isotherm lies at 1 km depth. Past x_0, isotherms deepen and the lithosphere thickens as a function of the distance squared, reaching a depth of h_1 over a lateral distance of 1 km. Farther from the axis we assign square root of distance isotherm deepening with coefficient *s*, simulating effects of conduction.

[18] We assume that prior to the ridge jump, the axial high evolved under steady state thermal conditions such that its morphology was similar to the EPR high near 8°S. We then modify this thermal and melt structure in several steps to simulate the ridge jump. Changes in temperature and melt structure, and thus associated stresses, lead to corresponding plate deflections and gravity anomalies.

3.3. Abandoned Ridge

[19] We model deflections arising from the cessation of spreading, the solidification of melt and the cooling of surrounding crust at an axial high. We start with a steady state model of a "typical" axial high and its associated thermal, magmatic, and stress structure, assumed to be symmetric about the axis. To simulate the cessation of spreading, we first assume that the plate is continuous at the axis. Subsequent deflections of a continuous plate are modeled by shifting the axial boundary conditions to a distance far from axis of symmetry (50 km for model runs

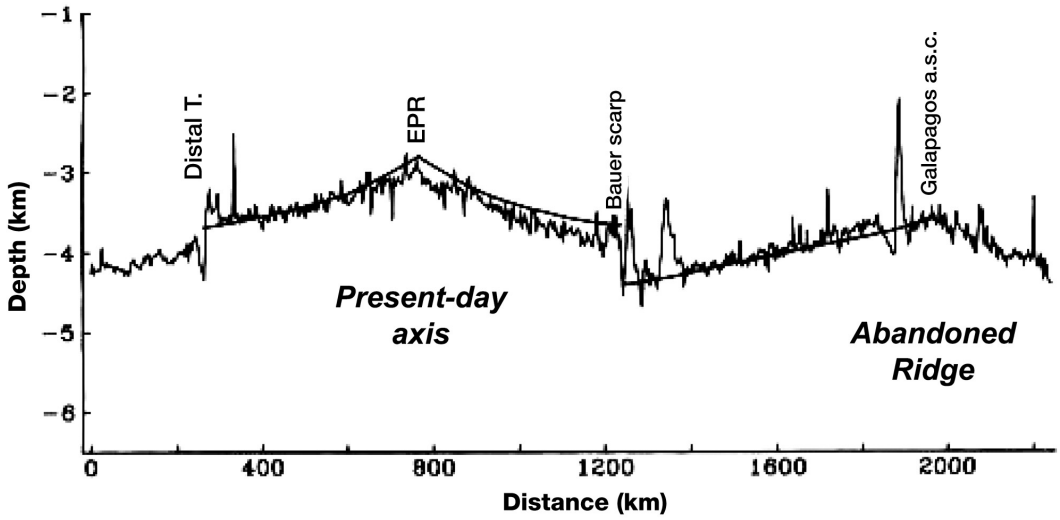

Figure 4. Bathymetric profile across the East Pacific Rise at 7°S, with the Galapagos abandoned spreading ridge at 12°S. Limited magnetic data suggest that the Galapagos ridge was abandoned at ~6.5 Ma. The smooth line is a depth versus age curve following *Parsons and Schlater* [1977]. From *Mammerickx and Sandwell* [1986].

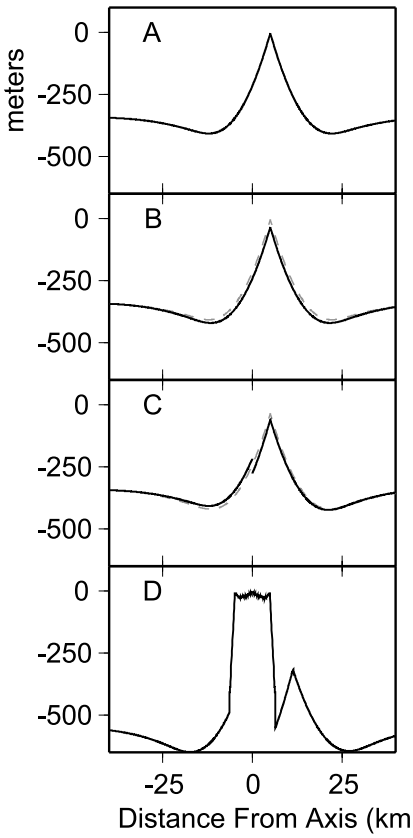

Figure 5. Model sequence of the ridge jump near 15°39′N. (a) Steady state case before the jump. (b) Cooled abandoned ridge (solid) and steady state ridge (dashed). (c) Break initiated 5 km from previous axis. (d) Accretion begins at new locale, with ~300 m increase in accretion level.

below), where they will have little effect on the deflections near the abandoned axis. We then apply a densification load arising from melt solidification and lithospheric cooling at the abandoned axis:

$$\Delta q_a(x) = \int_0^{h_{1200}} \rho_c g \alpha \Delta T(x,z) dz + \phi(\rho_c - \rho_m) g \Delta h_m(x),$$

where $\Delta T(x, z)$ is the change in temperature the region experiences, $h_{1200}(x)$ is the depth to the 1200°C isotherm in the final temperature distribution, ρ_c and ρ_m the density of the crust and melt, respectively; ϕ is the percentage of melt present over a column of height $h_m(x)$, defined as the distance between h_{1200} and the base of the crust, here taken to be 6 km (if h_{1200} is deeper than the base of the crust, $h_m(x) = 0$). $\Delta h_m(x)$ is then defined as the change in this height as the plate cools.

[20] The magnitude of the load will depend on the difference between the initial and final thermal/magmatic structure. The final structure is determined as follows: We assume that all melt solidifies. We then assume that within the region where quadratic "cooling" occurs, that the 1200°C isotherm lowers so that it is at a constant depth there. Final temperatures still increase linearly with depth, and are laterally constant beneath the axis. Note that as the plate cools, the 700°C isotherm deepens and the plate thickness thus increases. We assume that lithosphere accreted at the bottom of the plate is initially stress free. Because of possible nonlinear effects of changing lithosphere strength with cooling, we apply the load in increments, and examine the effects of different increment sizes.

3.4. Breaking Older Stressed Lithosphere

[21] Before ridge spreading can begin in a new location, the lithosphere must break there. The accretion history and associated changes in curvature of the ridge will create stresses within the plate where the break is to occur. Upon breaking, the release of this stress has an associated moment and shear force, which will cause the plate to deflect.

[22] To simulate breaking of old lithosphere, we begin with the steady state model deflection, lithosphere thickness, and stress state. As with the abandoned ridge scenario, we first assume that the ridge is continuous at the axis and all properties are symmetric about the axis. We can also break a plate which has already experienced cooling and melt solidification at an abandoned ridge to one side of the axis.

[23] A discontinuity is assigned to the point on the flank where the break is to take place, and different solutions for two new separate plates are modeled. The moment and shear force associated with the stress state at that location ($M = \int \sigma(x, z) z dz$; $V = dM/dx$, respectively), are applied as boundary conditions to the stressed plates, and the resulting changes in deflection are added to the previous deflection. Temperature and melt structures are kept constant, so $\Delta q = 0$.

3.5. Spreading and Accretion at the New Location

[24] After a plate has been broken, spreading and accretion can begin. New material is assumed to rise to a level defined by local isostasy. This level depends on the density distribution of material near the axis, and will thus depend on thermal conditions, melt content, and the depth at which material ponds in an axial magma chamber. Ridge jumps often occur in plume-influenced areas, and a new locus of spreading is likely to have temporally varying thermal and melt conditions. We thus depart from previous models by allowing the level of accretion, which is a model boundary condition, to differ from that of the abandoned ridge, and move up and down as the plate spreads.

[25] Conditions that will cause the level of accretion to vary are changes in temperature or melt content by affecting the density of material at the axis, but also the depth of the magma chamber. A deeper magma chamber can actually lead to a rise in accretion level as melt is generally buoyant compared to surrounding solidified rock, and the greater the column of melt, the higher it must rise so that its sum density matches that of the surrounding rock. This scenario, however, assumes that there is enough melt available to rise to the level of local isostasy.

[26] New material has an associated thermal structure and thickness as it attaches to older adjacent material. As newly accreted material moves away from the axis, it cools and melt beneath it solidifies, creating densification loads on the

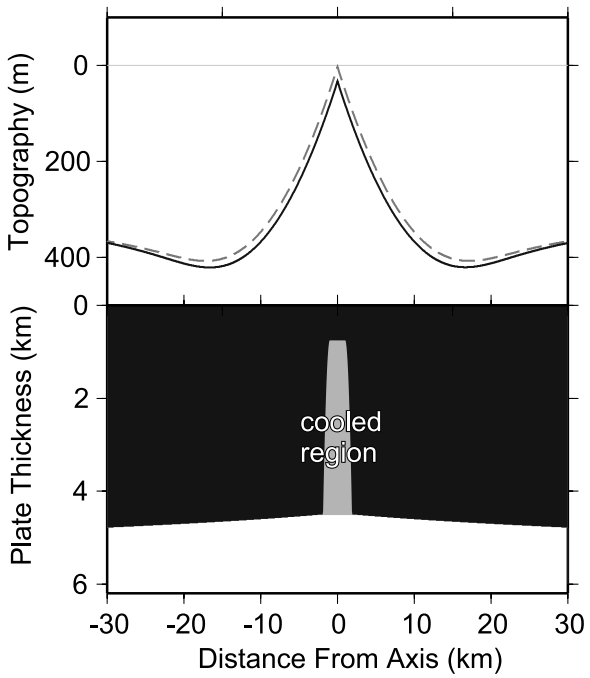

Figure 6. Model of deflections at an abandoned ridge. Parameters for steady state model are as in the work by *Shah and Buck* [2003], using the sample solution fitting topography at 8°S where $h_1 = 6$ km, $x_0 = 1$ km, melt percent is 30%, and $f = 0.5$, i.e., 50% of the depth to the 1200°C isotherm is fixed at 200°C (hydrothermal cooling effects). (top) Topography of the steady state model (gray dashed line), before abandonment and after cooling and solidification (black line). (bottom) Plate thickness (700° isotherm) before (black) and after (gray) cooling.

plate. The weight of each column is defined as a function of distance

$$q_c(x) = \int_0^{h_{1200}} g\rho_c\alpha_v(T(x,z) - T_m)dz + \phi(\rho_c - \rho_m)gh_m(x).$$

Deflections are then determined via equations (1)–(3).

4. Results

[27] Figure 5 provides a summary illustration of the steps of the ridge jump model.

4.1. Abandoned Ridge

[28] We began with a steady state model using the temperature and melt structure used by *Shah and Buck* [2003] to simulate topography at the EPR at 8°S (Figure 6). Crustal melt was solidified and the axial region cooled to create laterally uniform temperatures over a distance of 3 km from either side of the axis. Solidification and cooling have little affect on topography, with over 300 m of the axial high remaining. This occurs because the associated deflection is that of a strong plate: prior to cooling, stresses have mostly filled the yield strength envelope, but as the ridge cools, the plate bends in the opposite direction, stresses move away from the yield strength envelope, and the effective elastic plate thickness is several kilometers, close to that of the thermally defined lithosphere. The stronger plate has a greater flexural wavelength, causing deflections to be of smaller amplitude and spread over greater distances. The fact that the ridge has been "mended," i.e., the cooling load is applied to a continuous rather than plate, also implies longer wavelength deflections. A high remaining at the abandoned axis thus arises naturally from the mending and cooling process, and does not require any low-density material in order to persist.

4.2. Breaking Lithosphere

[29] Figure 7 shows results of breaking old, stressed lithosphere at different parts of the plate. For illustrative purposes, we have included both plastic and elastic models. In each of these cases, the release of moment has the effect of pushing the ridge upward. The shear stress creates an offset between the two sides of the break. Shear stresses are greatest near the axis (where the stresses and thus the moment change most dramatically), and decrease away from the axis.

[30] For a break situated far from the axis, the elastic case predicts deflections which near 50% of the relief of the original high. When plastic yielding effects are considered, however, there is almost no deflection because much of the stress has been lost due to yielding, illustrating the effects of the plastic formulation. This implies that to create new topography at a ridge break, an additional process such as a variable accretion level must be present to create the relief

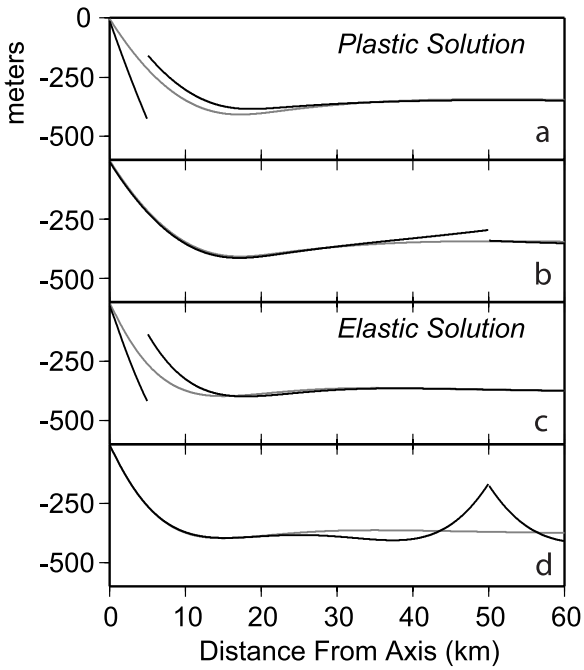

Figure 7. Breaking of a stressed ridge at (a) 5 km and (b) 50 km from the axis for models with plastic yielding. Temperature and melt structure as in Figure 6. (c) and (d) Deflections using elastic models, for best fit solutions of *Shah and Buck* [2001]. Gray lines show topography before breaking, and black lines show topography after breaking.

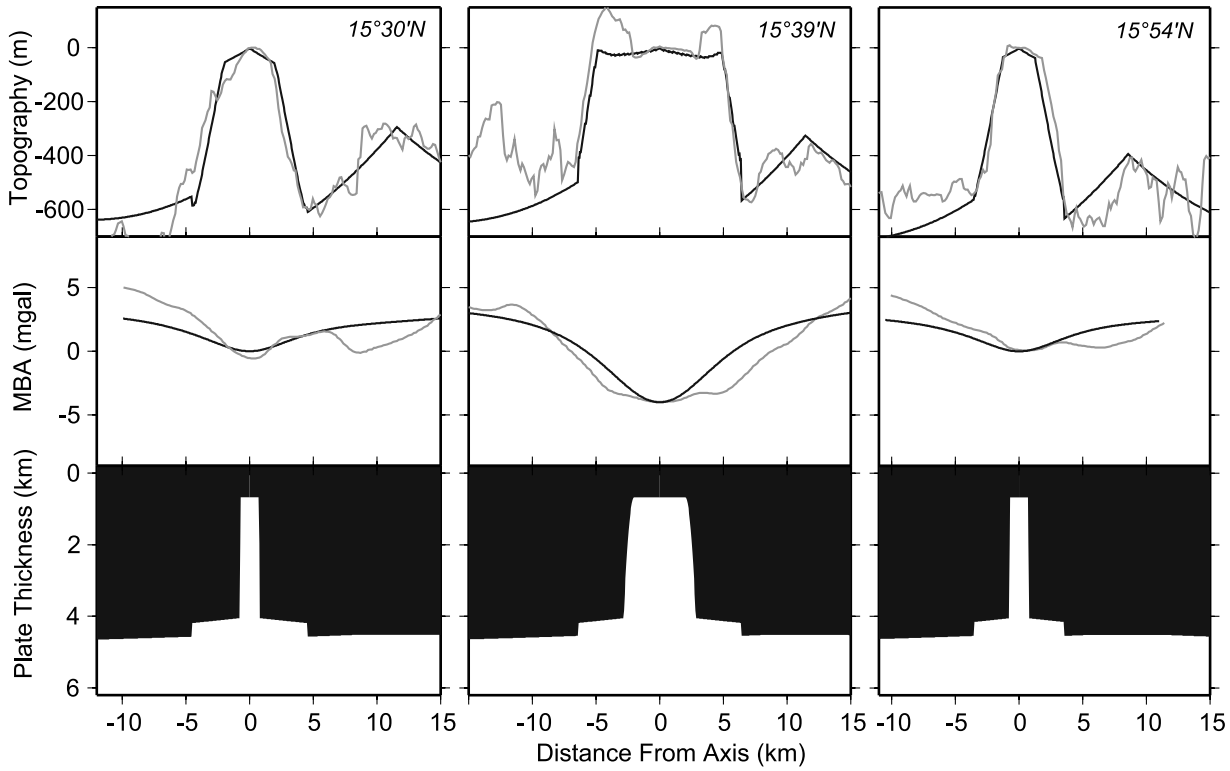

Figure 8. Model fits to cross sections of the steep-sided high between 15°N and 16°N using the ridge jump model. (top) Bathymetry data shifted to zero at the present-day axis (gray lines) and the model topography fit (black lines). (middle) Mantle Bouguer anomaly shown in Figure 1 (gray line) and gravity anomaly associated with the model crustal thermal structure (black line). (bottom) Regions below 700°C (shaded area), representing the elastic plate thickness. New temperature and melt parameters are as in Figure 6 except x_0 = 2 km for the 15°39′N profile and 0.7 km for the other profiles, also s = 8 $m^{1/2}$, and f = 0.35.

observed at a new high, especially if the break is far from the original axis.

4.3. Accreting Lithosphere at the New Break

[31] We combined the processes of ridge abandonment, lithospheric breaking, and accretion at a new location, to model topography and the associated gravity anomaly at three areas, 15°54′N, 15°39′N, and 15°30′N (Figure 8). These areas were chosen because of their marked difference in axial high width and mantle Bouguer anomaly character. Parameters such as percent melt in the lower crust and degree of hydrothermal cooling in the final profiles were kept the same for all cases.

[32] The primary differences in the three model solutions are the final plate thickness distributions and the history of accretion level, i.e., the level representing local isostasy (Figure 9). In each case, the solutions start with an accretion level below that of the ridge before the jump which quickly ramps up to several hundred meters higher than that level, producing the high's steep slopes. Near the center of the segment, the accretion level rises much sooner than that to the north or south, creating the different axial high widths. In this area, there also appears to be a subsequent gradual decrease yielding a relatively wide, flat top.

[33] Near the axis, the associated thermal and melt structures generally fit the amplitude of the observed gravity data anomalies. The wide low-density region near the center of the segment increases the magnitude of the Bouguer anomaly there, generating the observed bull's-eye shape. There is some misfit for to the gravity profiles, particularly below the abandoned ridge. It seems that there may be some residual thermal anomaly at the abandoned ridge site and that the area completely cooled. The residual anomaly is very small however, less than 2 mGal. Its limited cross-axis extent (<5 km) suggests that its source is within the crust. To the west, the long-range rate of cooling (for distances greater than a few kilometers from the axis) may be slightly underestimated, observable in the northern and southern profiles. Near the center of the segment, the Mudskipper seamounts to the west dominate off-axis cooling trends there.

4.4. Continued Spreading at a New Ridge

[34] Figure 10 shows a sequence of cases where we continue accretion under steady state conditions, i.e., constant temperature, melt structure, and accretion level, for a distance of up to 50 km after the ridge jump has occurred. Here we assume that the accretion level is the same as that of the abandoned ridge. The final axial high is more like that observed at 8°S. Where the ridge jump occurred, however, the steep slopes that initially bounded the new high remain. These slopes may be compared to bathymetry

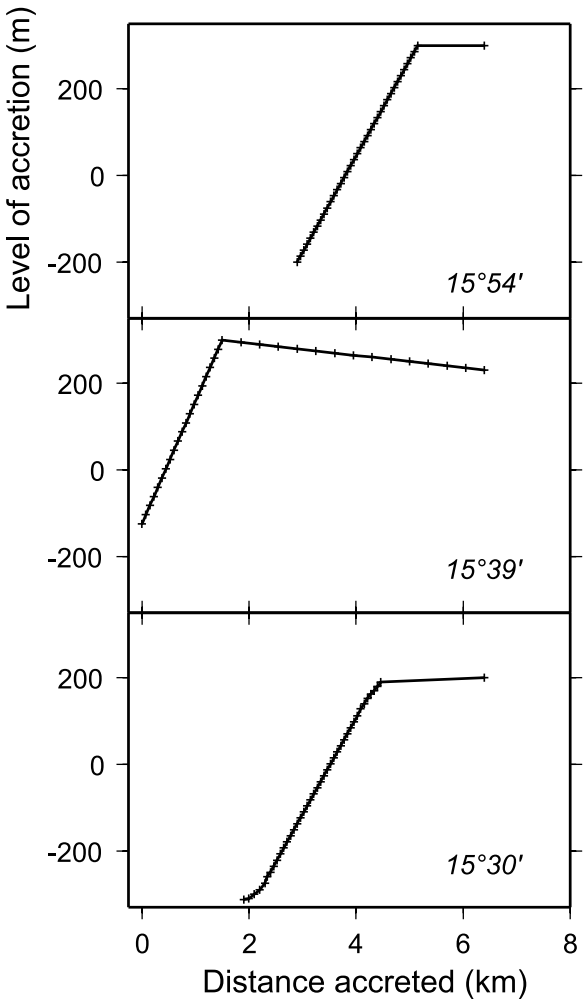

Figure 9. Variations in the level of accretion for models shown in Figure 8 as a function of distance accreted. Zero level corresponds to a depth of 2500 m, assumed to be the axial depth of the original high (rising 400 m above the surrounding flanks).

observed at 7°N by *Mammerickx and Sandwell* [1986], shown in Figure 4.

5. Discussion

5.1. Abandoned Ridge

[35] The region exhibits relief of several hundred meters at the site believed to be an abandoned ridge, yet gravity data do not indicate a narrow zone of buoyant material great enough to support this relief. While gravity data suggest that there is some residual thermal anomaly in the region, the models indicate that the axial high topography will persist even when this region has eventually cooled entirely.

[36] The remaining relief appears to be a direct consequence of plate cooling and strengthening. Although the source of buoyancy supporting the center of the high decreases, the increased plate strength causes the response to densification to be spread over a wider region. There is some reduction in height due to cooling, but most of the original topography remains. We note that numerous other models of axial high topography [e.g., *Madsen et al.*, 1984; *Kuo et al.*, 1986; *Wang and Cochran*, 1993; *Eberle and Forsyth*, 1998] assume that the crust cools and lithosphere thickens very slowly with distance from the axis. Analogous cooling and solidification loads applied to these models (or stress relief moments, in the case of *Eberle and Forsyth* [1998]) will act on relatively thin lithosphere, and will substantially reduce the vertical topography of the abandoned ridge. Indeed, it may be very difficult to parameterize these models in a way that will result in substantial abandoned axial high topography.

[37] The abandoned axial high near 16°N is somewhat blocky and irregularly shaped compared to the gentle slopes of the EPR near 8°S. This may reflect the shape of original spreading center, or may represent tectonic deformation associated with cooling of the lithosphere. To date, there is not enough information available to determine the exact cause of this shape, and the models are not designed to address this. Indeed, thermal conditions before the ridge jump may have been somewhat different from those at 8°S, the model solution that was used as input to the cooling model. However, the models show how abandoned ridge topography can persist without supporting buoyant material, as long as there is significant lithospheric thickening asso-

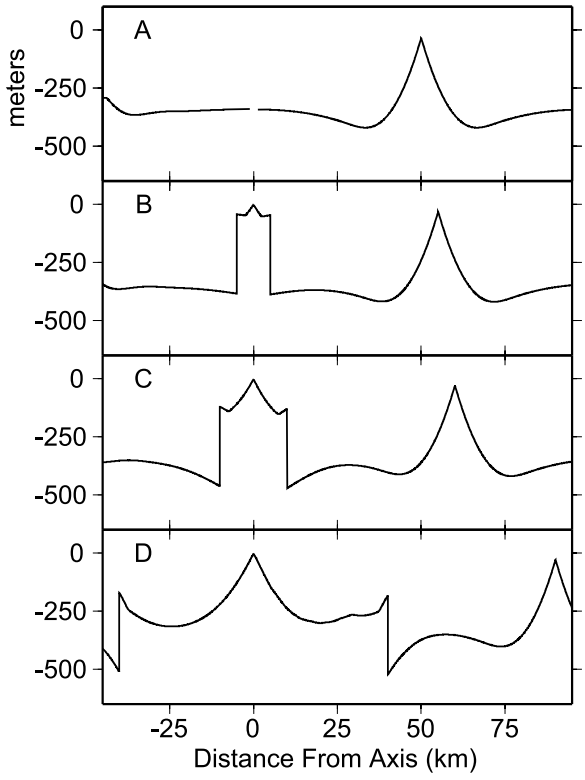

Figure 10. Model sequence for a ridge jump of 50 km with a constant level of accretion equal to that of the abandoned ridge. Model conditions for initial state and cooling of the abandoned ridge are the same as in Figure 6. (a) Break initiated 50 km from previous axis (comparable to Figure 5c). (b) Topography after spreading a half distance of 5 km (comparable to Figure 5d). (c) Topography after 20 km total spreading. (d) Topography after 40 km total spreading. Temperature and melt are as in Figure 8, segment 15°39′N but with $s = 5\ m^{1/2}$.

ciated with cooling and melt solidification. This model should thus still apply for mildly different preabandonment thermal conditions (as might be expected at other abandoned axial highs).

5.2. Steep Slopes Bounding the High

[38] For steady state flexural models to reproduce the steep slopes observed at this segment, the effective elastic plate thickness would have to be as thin as ~200–350 m past distances of 4–5 km from the axis. Such thin lithosphere seems highly unlikely for several reasons. Abyssal hills, usually attributed to faulting, reach heights of 100–200 m at such distances [e.g., *Goff*, 1991]. Nearly all models published to date which assume that the axial high is the result of the flexural response of the lithosphere require effective elastic thicknesses that are thicker than a few hundred meters at a distance of several kilometers from the axis [*Madsen et al.*, 1984; *Wang and Cochran*, 1993; *Kuo et al.*, 1986; *Shah and Buck*, 2001, 2003]. We are better able to reproduce the steep slopes by assuming they are constructional, so that the steepness of the slopes depends less on local lithospheric strength and more on thermal and/or magmatic conditions at the ridge axis at the time that material was formed and accreted.

[39] This constructional model for the development of a new axial high may also apply to propagation of an existing ridge. The growing end of propagating ridges on the EPR are marked by narrow steep sided axial highs [e.g., *Scheirer and Macdonald*, 1993]. We speculate that this may result from lateral delivery of magma from the old to the new sections of the ridge and accretion of that magma at a level above that of the surrounding surface of the oceanic crust.

5.3. Changes in Accretion Levels

[40] We find that by allowing variability to the depth at which new material accretes, the morphology of the axial high will respond in kind. Accretion levels at 15°N start off lower than that of the abandoned ridge, increase rapidly, and then taper off (near the center of the segment, they seem to decrease slightly). From variations in the width of the high, we infer that the increase in accretion level first occurred near the center of the segment, and then spread to the south, and then north, in the latter case possibly influencing segmentation boundary migration there.

5.3.1. Comparison to Layer 2A Thickness

[41] A rapid rise in accretion level is consistent with observed variations in extrusive layer thickness inferred from seismic layer 2A (Figure 2): if melt rises to depths shallower than older lavas, more extrusive rock will be produced as it cools. Along the slopes of the high, layer 2A is typically 300–400 m thick, but in some areas near the base of these slopes it is over 600 m thick. We infer that increased lava outpourings flowed down such steep slopes and gathered near the base of the high. Near the segment center, the "bat ears," which appear to be composed of extrusives, may indicate an area of pileup where lavas did not flow downhill.

5.3.2. Conditions Leading to Rapid Changes in Accretion Level

[42] Changes in the accretion level reflect temporal changes in the density structure at the axis through the local isostasy assumption. We consider two conditions which may contribute to such changes. Variations in the thermal structure at the axis will have a direct bearing on the density structure there. In the first stages of spreading, accretion levels are low (Figure 9), suggesting that conditions were generally cooler than at the previous ridge site when the abandoned ridge was active. The ridge would then have warmed rapidly, creating the steep slopes of the high. The accretion level reaches a depth that is ~200 m higher than that of the abandoned ridge, suggesting that conditions are now warmer and/or more magmatic than at the previous spreading site.

[43] Changes in the level of accretion can also be affected by the depth of the axial magma chamber because of the difference in density between melt and surrounding rock; a deeper magma chamber can actually lead to a greater amount of extrusive rock [see *Buck et al.*, 1997]. This argument follows by comparing density columns above the magma chamber: for example, assuming local isostasy, melt at 2700 kg/m^3 in a chamber at 6 km depth overlain with surrounding rock with a bulk density of 2870 kg/m^3 and water with density 1000 kg/m^3 will rise 600 m higher than that rock (6000 m × 1870 kg/m^3 = (6000 + 600) m × 1700 kg/m^3). On the other hand, melt from shallower magma chamber, say at 1 km depth, would only rise 100 m higher than the surrounding rock (1000 m × 1870 kg/m^3 = (1000 + 100) m × 1700 kg/m^3). This argument requires, however, that a deep axial magma chamber, often associated with cooler thermal regimes, be fed substantial amounts of melt in order for lavas to reach such heights. While such a scenario may seem improbable at a "cooler" ridge axis, a new locus of spreading may very likely experience rapid changes in thermal and/or magmatic conditions. Such a deep magma chamber, however, is not likely to persist as the region warms, and this contribution to an increasing accretion level would eventually abate. We note that the present-day axial magma chamber is relatively shallow, at ~1 km depth.

5.3.3. Shallow Depth of the New Ridge Axis

[44] The new ridge axis sits 600 m above surrounding flanks, compared to 400 m for most axial highs. This 50% increase in height suggests that some additional amount of low-density material is present below the ridge axis. The relief of the mantle Bouguer anomaly is not large enough to account for this as melt if we assume that the source lies within the crust (we have assumed 30% melt in lower crust, which is somewhat high compared to earlier EPR 8°N models). The higher topography does not appear to be due solely to a relative increase in crustal thickness along the new ridge axis. For example, a crustal thickness increase of 1 km along the axis would create a 10–15 mGal mantle Bouguer anomaly low along most of the length of the axis, which is not observed. It thus seems likely that a broad range of low-density mantle material causes the axial high to "float" at more shallow depths, possibly aided by the presence of slightly thicker crust. Such variations can be quantified roughly assuming local isostasy: a 200 m difference in accretion level (and thus water depth) can be achieved with a ~720-m-thick mantle melt density anomaly, equivalent to, for example, 10% melt over a ~7.2 km column, (assuming density contrasts of 1800 kg/m^3 for crust and water, and ~500 kg/m^3 for mantle versus melt). We speculate as to whether low-density mantle material facili-

tated the ridge jump process, noting that the present-day spreading ridge at the EPR near 7°S also sits several hundred meters higher than the abandoned Galapagos spreading center (Figure 4).

5.4. Bull's-Eye Bouguer Anomaly

[45] The 15°25′N–16°N area is marked by a mantle Bouguer anomaly bull's-eye pattern. At the Mid-Atlantic Ridge, these patterns are typically attributed to variations in crustal thickness [e.g., *Kuo and Forsyth*, 1988]. Such an interpretation poses a difficulty at this part of the East Pacific Rise, however, since one would expect corresponding undulations in axial depth. We propose that the average density directly beneath the axis is fairly uniform along axis but that the width of low-density material varies, as indicated in the plate thickness profiles in Figure 8. A wide region of higher temperatures and crustal melt near the segment center can then produce a bull's-eye pattern without affecting along-axis depth. Additionally, magma may build topography up to a nearly constant level along the length of the axis by along-axis diking and extrusive flow, as the extremely level along-axis depth does suggest some along-axis "communication."

6. Summary

[46] Steady state axial high models are developed to simulate ridge jumps. The mechanical processes modeled are (1) cessation of ridge spreading and cooling of the ridge axis (the increasing strength of the lithosphere causes a fossil high to remain without requiring buoyant support from low-density material in the crust or mantle), (2) the breaking apart of old lithosphere, (3) the construction of a high at the new ridge axis which may have relatively steep slopes (the shape of the high depends strongly on the way thermal and magmatic conditions develop at the new locale), and (4) continued spreading at the new ridge axis (the steep slopes marking the constructional high remain, forming scarp-like topography off-axis similar to that observed at the sites of other older ridge jumps).

[47] Using this model to fit topography and gravity data at the EPR near 15°25′–16°N, where previous magnetic field and bathymetry data suggest that a ridge jump took place, we infer the following:

[48] 1. After ridge abandonment, a break occurred in old lithosphere about ~5 km west of the axis. A fossil high remains at the site of the old axis.

[49] 2. At the new break, the level of accretion of new material increased rapidly, creating steep constructional slopes to the new axial high. We propose that the region started off with a cooler thermal structure and deep magma chamber, but temperatures and melt supply increased rapidly. This rapid temperature increase, as well as higher overburden pressure associated with a deep magma chamber, both contributed to the rapid increase in accretion level, as well as a sharp increase in extrusive lava outpourings, as suggested by layer 2A thickness variations.

[50] 3. Magmatic activity and the buildup of an axial high appear to have initiated near 15°42′N, and gradually propagated south and then north along axis. Material is currently emplaced along axis at a level 200–300 m higher than before ridge abandonment.

[51] 4. The axial high is widest near the center of the segment, near 15°42′N, and is best modeled with a wider crustal melt zone than regions to the north and south. Gravity data exhibit a "bull's-eye" mantle Bouguer anomaly centered near this area, but the depth of the axis remains nearly constant along the length of the segment, indicating crustal thickness variations are an unlikely source of the bull's-eye anomaly. Varying the width of a crustal melt zone below the axis, but not the percentage of melt below the axis, is consistent with both constant along-axis depth and a bull's-eye mantle Bouguer anomaly.

[52] **Acknowledgments.** We thank Suzanne Carbotte and Milene Cormier for helpful discussions regarding the 15°–16°N study area. We also thank Suzanne Carbotte for sharing gravity and seismic layer 2A data from the region. We thank two anonymous reviewers and an Associate Editor for insightful comments regarding the manuscript. This project was partly inspired by a RIDGE Summer School on plume-ridge interaction. This work was funded by grant OCE-01-37293 and an NRC Postdoctoral Research Associateship. Lamont contribution 6928.

References

Bodine, J. H., M. S. Steckler, and A. B. Watts (1981), Observations of flexure and the rheology of the oceanic lithosphere, *J. Geophys. Res.*, *86*, 3695–3707.

Buck, W. R. (2001), Accretional curvature of lithosphere at magmatic spreading centers and the flexural support of axial highs, *J. Geophys. Res.*, *106*, 3953–3960.

Buck, W. R., S. M. Carbotte, and C. Z. Mutter (1997), Controls on extrusion at mid-ocean ridges, *Geology*, *25*, 935–938.

Carbotte, S., and K. C. Macdonald (1992), East Pacific Rise 8°–10°30′N: Evolution of ridge segments and discontinuities from SeaMARC II and three-dimensional magnetic studies, *J. Geophys. Res.*, *97*, 6959–6982.

Carbotte, S., A. Solomon, and G. Ponce-Correa (2000), Evaluation of morphological indicators of magma supply and segmentation from a seismic reflection study of the East Pacific Rise 15°30′–17°N, *J. Geophys. Res.*, *105*, 2737–2759.

Cochran, J. R., J. C. Sempéré, and SEIR Scientific Team (1997), The Southeast Indian Ridge between 88°E and 120°E: Gravity anomalies and crustal accretion at intermediate spreading rates, *J. Geophys. Res.*, *102*, 15,463–15,487.

Crawford, W. C., S. C. Webb, and J. A. Hildebrand (1999), Constraints on melt in the lower crust and Moho at the East Pacific Rise, 9°48′N, using seafloor compliance measurements, *J. Geophys. Res.*, *104*, 2923–2939.

Dunn, R. A., and D. T. Toomey (2000), Three-dimensional seismic structure and physical properties of the crust and shallow mantle beneath the East Pacific Rise at 9°30′N, *J. Geophys. Res.*, *105*, 23,537–23,555.

Eberle, M. A., and D. W. Forsyth (1998), An alternative, dynamic model of the axial topographic high at fast spreading ridges, *J. Geophys. Res.*, *103*, 12,309–12,320.

Eberle, M. A., D. W. Forsyth, and E. M. Parmentier (1998), Constraints on a buoyant model for the formation of the axial topographic high on the East Pacific Rise, *J. Geophys. Res.*, *103*, 12,291–12,307.

Forsyth, D. W., D. S. Scheirer, and the MELT Seismic Team (1998), Imaging the deep seismic structure beneath a mid-ocean ridge: The MELT experiment, *Science*, *280*, 1215–1218.

Goff, J. A. (1991), A global and regional stochastic analysis of near-ridge abyssal hill morphology, *J. Geophys. Res.*, *96*, 21,713–21,737.

Hey, R. N. (1977), A new class of "pseudo faults" and their bearings on plate tectonics: A propagating rift model, *Earth Planet. Sci. Lett.*, *37*, 321–325.

Hey, R. N. (1979), Evidence for spreading outer jumps from fine-scale bathymetry and magnetic anomalies near the Galapagos Islands, *Geology*, *7*, 504–506.

Hirth, G., J. Escartin, and J. Lin (1998), The rheology of the lower oceanic crust: Implications for lithospheric deformation at mid-ocean ridges, in *Faulting and Magmatism at Mid-Ocean Ridges*, *Geophys. Monogr. Ser.*, vol. 106, edited by W. R. Buck et al., pp. 291–323, AGU, Washington, D. C.

Kuo, B.-Y., and D. W. Forsyth (1988), Gravity anomalies of the ridge-transform system in the South Atlantic between 31 and 34.5°S: Upwelling centers and variations in crustal thickness, *Mar. Geophys. Res.*, *10*, 205–232.

Kuo, B. Y., D. W. Forsyth, and M. Parmentier (1986), Flexure and thickening of the lithosphere at the East Pacific Rise, *Geophys. Res. Lett.*, *13*, 681–684.

Langmuir, C. H., J. F. Bender, K. E. Donnelly, S. B. Shirey, M. Cormier, and E. Baker (1998), Sr, Nd, and Pb isotopic constraints on the relationship between EPR and seamount volcanism in the pacific: 15–19°N, *Eos Trans. AGU*, *79*(45), Fall Meet. Suppl., F832.

Lin, J., G. M. Purdy, H. Schouten, J.-C. Sempere, and C. Zervas (1990), Evidence from gravity data for focused magmatic accretion along the Mid-Atlantic Ridge, *Nature*, *344*, 627–632.

Madsen, J. A., D. W. Forsyth, and R. S. Detrick (1984), A new isostatic model for the East Pacific Rise crest, *J. Geophys. Res.*, *89*, 9997–10,015.

Magde, L. S., R. S. Detrick, and the TERA Group (1995), Crustal and upper mantle contribution to the axial gravity anomaly at the southern East Pacific Rise, *J. Geophys. Res.*, *100*, 3747–3766.

Mammerickx, J. (1984), The morphology of propagating spreading ridges: New and old, *J. Geophys. Res.*, *89*, 1817–1828.

Mammerickx, J., and D. Sandwell (1986), Rifting of old oceanic lithosphere, *J. Geophys. Res.*, *91*, 1975–1988.

Morgan, W. J. (1978), Rodriguez, Darwin, Amsterdam, . . ., A second type of hotspot island, *J. Geophys. Res.*, *83*, 5355–5360.

Parsons, G., and J. G. Schlater (1977), Ocean floor bathymetry and heat flow, *J. Geophys. Res.*, *82*, 803–827.

Scheirer, D. S., and K. C. Macdonald (1993), Variation in cross-sectional area of the axial ridge along the East Pacific Rise: Evidence for the magmatic budget of a fast-spreading center, *J. Geophys. Res.*, *98*, 7871–7885.

Schilling, J.-G. (1985), Upper mantle heterogeneities and dynamics, *Nature*, *314*, 62–67.

Schilling, J.-G. (1991), Fluxes and excess temperatures of mantle plumes inferred from their interaction with migrating mid-ocean ridges, *Nature*, *352*, 397–403.

Sempéré, J. C., J. R. Cochran, and SEIR Scientific Team (1997), The Southeast Indian Ridge between 88°E and 118°E: Variations in crustal accretion at constant spreading rate, *J. Geophys. Res.*, *102*, 15,489–15,505.

Shah, A. K., and W. R. Buck (2001), Causes for axial high topography, and the role of crustal thermal structure, *J. Geophys. Res.*, *106*, 30,865–30,879.

Shah, A. K., and W. R. Buck (2003), Plate bending stresses at axial highs and implications for faulting behavior, *Earth Planet. Sci. Lett.*, *211*, 343–356.

Sleep, N. H. (1992), Hotspot volcanism and mantle plumes, *Annu. Rev. Earth Planet. Sci.*, *20*, 19–43.

Small, C. (1995), Observations of ridge-hotspot interactions in the Southern Ocean, *J. Geophys. Res.*, *100*, 17,931–17,946.

Wang, X., and J. Cochran (1993), Gravity anomalies, isostasy, and mantle flow at the East Pacific Rise crest, *J. Geophys. Res.*, *98*, 19,505–19,531.

Weiland, C. M., and K. C. Macdonald (1996), Geophysical studies of the East Pacific Rise 15°–17°N: An unusually robust segment, *J. Geophys. Res.*, *101*, 20,257–20,274.

Wilson, D. S. (1992), Focused upwelling beneath mid-ocean ridges: Evidence from seamount formation and isostatic compensation of topography, *Earth Planet. Sci. Lett.*, *113*, 41–55.

W. R. Buck, Lamont-Doherty Earth Observatory, Columbia University, Palisades, NY 10964, USA.

A. K. Shah, Applied Signal Technology, 1555 Wilson Blvd., Arlington, VA 22209, USA. (ashah@ldeo.columbia.edu)